





Energy Storage Planning for Enhanced Resilience of Power Distribution Networks Against Earthquakes

Mostafa Nazemi , *Student Member, IEEE*, Moein Moeini-Aghtaie , *Member, IEEE*,
Mahmud Fotuhi-Firuzabad , *Fellow, IEEE*, and Payman Dehghanian , *Member, IEEE*

Abstract—Energy infrastructures are perceived continuously vulnerable to a range of high-impact low-probability (HILP) incidents—e.g., earthquakes, tsunamis, floods, windstorms, etc.—the resilience to which is highly on demand. Specifically suited to battery energy storage system (BESS) solutions, this paper presents a new resilience-driven framework for hardening power distribution systems against earthquakes. The concept of fragility curve is applied to characterize an earthquake hazard, assess its impact on power distribution systems, and estimate the unavailability of the network elements when exposed to extreme earthquakes. A new metric is defined to quantify the network resilience taking into account the uncertain nature of such HILP events. A linear programming optimization problem is formulated to determine the capacity and location of the BESSs for enhanced resilience against earthquakes. Efficacy of the proposed framework is numerically analyzed and verified through application to a real-world distribution power grid.

Index Terms—Battery energy storage system (BESS), earthquake, hardening, high-impact low probability (HILP), power distribution system, resilience.

NOMENCLATURE

A. Sets and Indices

τ	Index for the earthquake time of occurrence.
b, N_b	Index and the total number of BESSs.
i	Index for network islands.
k, K	Index and total number of line sections.
l_p, N_{l_p}	Index and total number of critical load points.
NI_s	Total number of islands in scenario s .
n	Index for the system operating state following an earthquake.
nd	Index for system nodes (substations).
s, N_s	Index and total number of scenarios.
T	Index for the time slots.

Manuscript received October 7, 2018; revised February 4, 2019; accepted March 16, 2019. Date of publication March 26, 2019; date of current version March 23, 2020. Paper no. TSTE-01001-2018. (*Corresponding author: Payman Dehghanian.*)

M. Nazemi and P. Dehghanian are with the Department of Electrical and Computer Engineering, George Washington University, Washington, DC 20052 USA (e-mail: mostafa_nazemi@gwu.edu; payman@gwu.edu).

M. Moeini-Aghtaie is with the Department of Energy Engineering, Sharif University of Technology, 11365-11155 Tehran, Iran (e-mail: moeini@sharif.edu).

M. Fotuhi-Firuzabad is with the Center of Excellence in Power System Management and Control, Department of Electrical Engineering, Sharif University of Technology, 11365-11155 Tehran, Iran (e-mail: fotuhi@sharif.edu).

Color versions of one or more of the figures in this paper are available online at <http://ieeexplore.ieee.org>.

Digital Object Identifier 10.1109/TSTE.2019.2907613

B. Parameters and Constants

$\alpha_{b,s,i}$	Binary parameter with 1 representing the BESS b in scenario s located in island i and 0, otherwise.
v_{dl_k}, γ_{dl_k}	Binary indicator of availability and unavailability of distribution line section k , respectively.
C^f	Fixed installation cost of the BESS (\$).
C^P, C^E	Variable installation cost of BESS reflecting power (\$/kW) and energy (\$/kWh) size, respectively.
\bar{C}	The marginal budget for BESS installation (\$).
CP_E	Cumulative probability of an extensive damage state (E) of the buildings following a seismic hazard.
Dis	The distance between the overhead lines and the nearby buildings.
$D_\tau^{t^e}$	Total system energy demand at the time interval starting at τ with the duration of t^e .
$E_{lp,t}^{t^e}$	Energy demand at load point lp during emergency time-interval t^e started at time slot t .
F_{dl_k}, F_{bl}	Failure of line section k and buildings, respectively.
G_a	Peak ground acceleration.
$L_{\tau,s,i,t}$	Total load in island i in scenario s at time slot t if an earthquake occurs at time τ (kW).
$L_{lp,t}$	Load demand at load point lp at time slot t .
LC	Critical load curtailment (kW).
P_n	Probability of a system operating state n following an earthquake.
p_τ	Probability of earthquake occurrence at time τ .
$P[x G_a]$	Cumulative probability of the system damage state $x \in \{N, Sl, M, E, C\}$.
P_x	Individual probability of the system damage state $x \in \{N, Sl, M, E, C\}$.
t^e	Emergency time duration.
u_{dl_k}	Unavailability of line section k under direct effect of an earthquake.
\bar{U}_{dL_k}	Expected unavailability of line section k under both direct and indirect effect of an earthquake.
λ	Rate parameter of an exponential function.
η_b^{dch}	Discharge efficiency of BESS b .
lg_{tot}	Total length of distribution lines (m).
lg_k	Length of line section k (m).

C. Functions and Variables

$E_{b,\tau,s,t}$	Energy level of BESS b in scenario s at time slot t if an earthquake occurs at time τ (kWh).
E_b^{max}	Maximum nominal energy level of BESS b (kWh).

$E_{b,\tau}^{max}$	Maximum energy level of BESS b if an earthquake occurs at time τ (kWh).
p_s	Probability of scenario s .
P_b^{max}	Maximum nominal discharge power rating of BESS b (kW).
$P_{b,\tau,s,t}^{dch}$	Discharge power of BESS b in scenario s at time slot t if an earthquake occurs at time τ .
RI	Resilience index.

I. INTRODUCTION

NATURAL disasters, e.g., floods, windstorms, tsunamis, and earthquakes, have been observed to impose potentially devastating and widespread striking effects on the nations critical energy infrastructures [1]. Among such high-impact low-probability (HILP) incidents, the occurrence of which has been trending higher in recent years, one can highlight the 2010 earthquakes and tsunamis in Nepal and Chile knocking power to many customers for several days [2], the 2012 Hurricane Sandy in the U.S. resulting in an extensive outage affecting 8 million customers with estimated \$75 billion economic loss [3], the 2016 Hurricane Hermine with approximately 8.5 million customer power outages and direct damage amounted to \$71.4 billion in the U.S. [4], the 2017 Hurricane Harvey in Texas causing 10,000 MW electricity outages to 291,000 people in the state [5], and the 2017 Hurricane Irma leading to a power outage of 6.7 million electricity customers in Florida accounting for 67% of all state customers [6]. According to [7], 58% of all the U.S. grid outages in the 10-year time interval from 2003 to 2012 are driven by the weather-caused HILP events resulting in an estimated \$18–33 billion annual loss. With an elevated incidence and severity, the resilience of the electricity delivery infrastructure and its capacity to withstand such outage-inducing HILP patterns has become more and more critical to peoples well-being and every aspect of our economy [8], [9].

Traditionally, power system planning and operations were centered on principle reliability metrics and known evaluation techniques [10]. Although reliability indices can well represent the system ability in best confronting the potential but credible failures (termed as security criteria), the focus was not on HILP incidents, resulting in an inability to efficiently capture the looming effects of severe patterns such as earthquakes and other HILP disasters [11]. Additionally, traditional power grids, designed based on the reliability principles, were primarily planned to be able to supply all load points during normal operating conditions, while load recovery and support in the face of extreme disasters was not a primary focus of concern [12]. In recent years, research and developments have been geared toward designing, planning, and operation of modern power grids that are not only secure and reliable in normal operating conditions and to the known and predictable threats, but also resilient against extreme and unpredictable HILP incidents [13]–[18]. The concept of power grid resilience has been defined and quantified in [12], [19]–[24] and future challenges for resilience are reviewed in [24]. Several strategies were suggested for delivering electricity to the end users safely, securely, and resiliently following natural hazards. Some efforts were focused on

microgrids as a solution for improved resilience [25]–[28]. Authors in [29]–[31] developed optimization models for load restoration in distribution systems during extreme events. Network hardening strategies, e.g., underground power lines, are discussed in [7]. The impacts of natural events on the equipment reliability attributes is focused in [13] and extensive weather-driven resilience analytics are developed in [32], [33].

Among different HILP disasters, earthquakes are the one most unpredictable class of hazards [34] which may lead to widespread disruptions of vital infrastructures. There are several research efforts in the literature that have studied the impact of seismic hazards on the power grid: [35] proposed a risk-based seismic model where a suite of earthquake scenarios and a corresponding set of consequential patterns on transmission lines and substations are defined to optimize the capacity expansion of transmission and generation sectors. Different upgrading strategies were introduced in [36] to decide on vulnerable nodes under different seismic scenarios. The criticality of electric components was evaluated in [37] via a resistance index during various earthquake conditions in Japan. A framework was proposed in [38] to assess the system resilience in terms of Energy not Supplied and Energy index of Unreliability following an earthquake and three adaptation strategies (e.g. robustness, redundancy, responsiveness) are evaluated for the northern Chilean electric power system. Similarly, the authors in [39] generated multiple earthquake scenarios using Monte-Carlo simulations to sample the earthquake intensity and location. In [40], [41], a seismic vulnerability assessment using network hierarchical decomposition is applied on the IEEE 118-bus test system which was stressed by uniformly and spatially generated earthquake scenarios. In [42], vulnerability of the interdependent European gas and electricity transmission networks was studied using a GIS-based probabilistic reliability model. A framework for seismic risk assessment in electric power systems was proposed in [43] with the focus on a probabilistically-weighted hazard scenario approach followed by the accessibility assessment of electric components. Reference [44] harnesses historic seismic events (e.g. 1971 San Fernando and 1994 Northridge earthquakes) to evaluate the seismic performance of the electric grid in the city of Los Angeles and assess the loss of connectivity using fragility curves. Similarly, [45] evaluated the degradation performance of the Los Angeles Department of Water and Powers (LADWPs) electric power system using 47 earthquake scenarios. Reference [46] identifies sequential failures of transmission network under severe earthquake hazards in the Los Angeles. In [47], [48], the seismic performance and vulnerability of the electric power system in the San Francisco Bay area following the 1989 Loma Prieta earthquake is evaluated. The loss of connectivity between substation, the failure probability of substations and transformers, and power imbalances in the system are evaluated in [49] considering a sample earthquake scenario with moment magnitude of 7.5. The authors in [50] presented an algorithm to evaluate the serviceability of water distribution systems and its interactions with the power grid following a scenario-based earthquake characterization. The authors in [51] collected a large damage dataset to develop fragility curves for a wide range of power equipment.

Only a few efforts can be found in the literature that comprehensively model and illustrate how the earthquake energy attenuates, which parameters affect the earthquake energy attenuation, how earthquake energy parameters (e.g., Peak Ground Acceleration) at the location of the power equipment can be assessed, how the earthquake energy can be quantified in terms of equipment fragility curves and consequently how the impact of seismic shocks on the power distribution lines can be mathematically modeled and quantified. In addition to a lack of effective resilience metrics [12], [22], the main challenge in many of the above efforts is the loose link and unfocused attention to the network fragility models to quantify its resilience against extreme disasters [13]. This paper is among the first efforts to address the above issues tailored to power distribution systems with the main goal of enhancing the system and equipment resilience.

Modern power distribution grids are furnished with massive proliferation of advanced smart grid technologies, e.g., electric vehicles, distributed energy resources, and Battery Energy Storage System (BESS), offering additional operational flexibility that can be harnessed for enhanced resilience during emergencies. Focusing on BESSs with exclusive features of high efficiency, fast response, and low maintenance costs, this paper suggests an analytical planning framework to harden the distribution grid with BESS and achieve a targeted emergency response and enhanced resilience. In this paper, the HAZUS model developed by the Federal Emergency Management Agency (FEMA) has been harnessed with the fundamental concept of fragility curves to achieve efficient analytics for impact assessment of earthquakes on power distribution grid resilience. Both direct and indirect effects of an extreme earthquake on distribution overhead lines are effectively characterized in this paper, where the former includes the power tower collapse (possibly resulting in disconnection of several customers), and the latter is concerned with collapse of the adjacent buildings on the power lines (increasing the overhead line unavailability). Different from the past research, our main contributions are highlighted as follows:

- *Seismic Hazard Characterization and Impact Assessment on Power Distribution Systems:* We develop analytical models that systematically characterize the seismic hazards and capture the vulnerability of distribution system elements to earthquakes. Centered on the fundamental concept of fragility curves, the effects of seismic forces on power distribution system elements—towers and overhead line sections—and the equipment unavailability due to both direct and indirect effects are quantified.
- *Optimization Model for BESS Sizing and Siting:* Mathematical linear-programming (LP) optimization formulations are derived to plan for distribution system hardening against earthquakes and investigate the BESS ability in boosting the network resilience.

The remainder of this paper is organized as follows. Section II presents an overall picture of the proposed framework. Seismic hazard characterization and vulnerability assessment models for distribution system elements are discussed in Section III. Section IV presents the proposed resilience-driven BESS planning algorithm in distribution networks. Section V elaborates the numerical analysis of

the proposed framework applied to a real-world distribution system, and Section VI concludes the paper at the end.

II. PROPOSED FRAMEWORK: BIG PICTURE

Figure 1 presents the overall architecture of the proposed three-stage framework as follows:

- *Seismic Hazard Modeling and Characterization:* Different seismic faults with high geological risks are first identified using historical earthquake catalogues. The potential seismic risk corresponding to each fault is estimated using the fundamental principles of geological and seismic engineering via which the highest seismic potential can be characterized. As the earthquake energy propagation and attenuation is highly dependent on the pattern the earthquake waves pass through, the soil type at the location of power distribution facilities (e.g., overhead lines) should be determined. In order to assess the seismic intensity at the location of power equipment, an analytical parameter, i.e., the attenuation relationship (AR), is characterized, based on which, critical seismic factors—e.g., peak ground acceleration (PGA)—are assessed. The main algorithmic process proposed for seismic hazard characterization is briefly summarized as follows:
 - 1) Estimation of the most probable earthquake magnitude (M_W) at the location of interest using historical earthquake catalogues.
 - 2) Determining the ground (soil) type at the location of interest.
 - 3) Estimation of a technical attenuation relationship suitably capturing the geotechnical characteristics at the location of interest.
- *Seismic Vulnerability Assessment:* A set of damage states are introduced highlighting the fact that different structures respond differently to a seismic force and, hence, unleash different vulnerability levels following the hazard. Five damage states (none, slight, moderate, extensive, and complete damage) for different line sections in distribution feeders are integrated with the fundamental principles of fragility curves to estimate the availability and the unavailability of distribution line sections under direct seismic effects (e.g. collapse of power towers) and indirect effects (e.g. collapse of the adjacent buildings on overhead distribution lines).
- *Resilience-Driven BESS Planning:* Restoration of critical load points, e.g., hospitals, water treatment systems, and military services, is a priority in the emergency response programs following an earthquake. This stage presents a grid hardening optimization problem for BESS siting and sizing in power distribution grids. The location of the BESS resources is found such that the curtailment of critical loads following an earthquake is minimal. A quantitative resilience metric is defined, based on which an LP optimization formulation and a solution algorithm are suggested to determine the optimal size of the BESSs across the network. Overall, instead of positioning the operator in a reactive mode in response to the aftermath of HILP

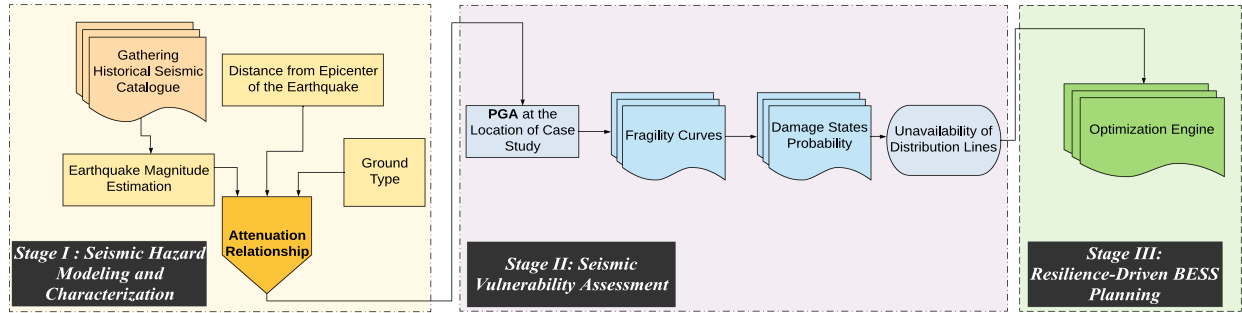


Fig. 1. Proposed framework: Big picture.

outages, the suggested formulation helps in hardening against the possible HILP-contingency outcomes, before the event happens.

The conceptual resilience performance of an engineered structure in the face of a hazard has been introduced in several studies [21], [22], [52]–[54]. According to Fig. 2, a HILP incident typically results in the system performance to degrade to a minimum level at t_{r1} . If the BESS units are deployed, it can be seen that not only is t_{r1} shifted with ΔT to limit the disruption time, but also the system performance would be improved by ΔP_D . One may then realize that hardening the distribution grid with BESSs results in an improved system resilience as the demanded critical loads will be supplied longer ($\Delta T = t_{r2} - t_{r1}$) during the disruption phase.

III. SEISMIC HAZARD CHARACTERIZATION AND VULNERABILITY ASSESSMENT

A. Earthquake Energy Transfer Model

In order to model how the released seismic energy of an earthquake attenuates, we employ probabilistic derivations to quantify the AR parameter. Principally, AR is defined for a specific geographical area to determine and analyze earthquake parameters in that area. Soil type, fault type, faults seismic potential, the length of a geological fault, and other geological parameters are among the inputs contributing to the AR derivation. In particular, AR characterizes a function between one earthquake characteristic and the other related parameters—e.g., seismic intensity, the distance between the equipment locations and the geological fault, etc.—. A general analytical form of the AR is formulated in (1) [55]:

$$\ln Y = a + F_1(M) + F_2(R) + F_3(P_x) + \epsilon \quad (1)$$

where, Y is one earthquake parameter such as G_a ; a is a constant; ϵ is a random error with mean value of zero and standard deviation of σ representing the uncertainty in Y . M is the earthquake intensity represented by Richter local magnitude, moment magnitude (M_W), etc.; R reflects the distance of the earthquake focus (hypocenter) to the location of interest. A number of methods have been proposed in different studies to determine the distance between the hypocenter of an earthquake and a location of interest. According to Fig. 3, the distance between a site of interest and the epicenter, the point on the Earth's surface

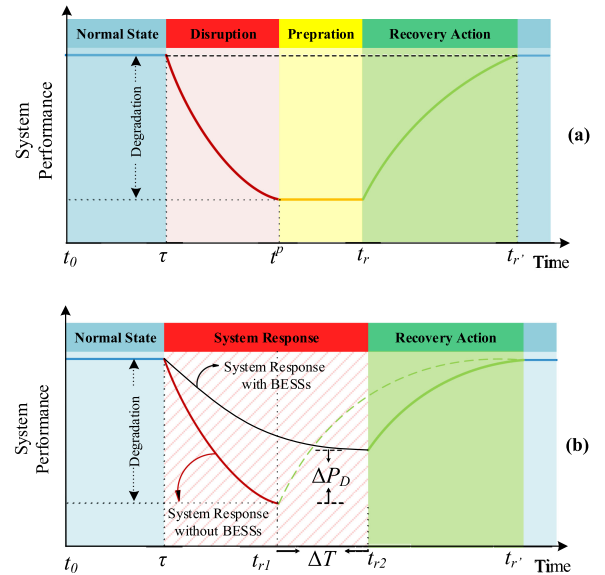


Fig. 2. (a) System transition states following a critical HILP disturbance: the disruption starts at τ and after a preparation interval ($t_r - t^p$), restorative actions help improving the degraded performance back to its normal condition within ($t_{r1} - t_r$). (b) Application of the proposed hardening framework to realize a more flexible system response to HILP events. t_{r1} is shifted with ΔT to limit the degradation and improve the system performance by ΔP_D .

directly above a hypocenter, is considered as R_{Epi} ; and P_x is the ground type assessed according to properties of the subsoil and shear wave velocities. The ground type affects all characteristics of the ground motion such as amplitude, frequency content and period. Note that the function Y characterizes a direct relationship with the earthquake intensity and an inverse relation with the distance from the geological fault.

B. Fragility Curve

In the context of this paper, fragility curves are established as statistical tools which represent the probability of exceeding a given (potential) damage state (or performance) during an earthquake as a function of PGA (G_a)—PGA represents the ground motion (preferably spectral displacement at a given frequency). Fragility curves can be generally derived by different approaches: (i) it can be empirically characterized utilizing the statistical representations and analysis of large data sets on

system elements failure records; (ii) it can be characterized through expert judgments; (iii) it can be experimentally characterized under a series of shocks applied with different intensity levels on a given structure; (iv) it can be analytically characterized through extensive simulation of the structure performance under different simulated shocks with different intensity levels; or (v) it can be characterized through a mixed combination of these approaches [13].

In order to model and assess the vulnerability of distribution line sections to a seismic hazard, the principle concepts of fragility curves are utilized, which *expresses the failure probability of a component as a function of seismic parameter* (e.g., PGA). Damage functions for system equipment are characterized in the form of lognormal fragility curves reflecting the probability of being in or exceeding a damage state for a given seismic parameter. Each fragility curve is defined by a median value of the PGA parameter and lognormal standard deviation (β) which correspond to the damage state thresholds and its variability [56]. The probability of residing in or exceeding a state of structural damage (d_s) is described as follows:

$$P[d_s|S_d] = \phi \left[\frac{1}{\beta_{d_s}} \ln \left(\frac{S_d}{\bar{S}_{d,d_s}} \right) \right] \quad (2)$$

where, S_d is spectral displacement and \bar{S}_{d,d_s} is its median value; β_{d_s} is the standard deviation corresponding to the natural logarithm of the spectral displacement at which a structure reaches the damage state threshold, and ϕ is the standard cumulative normal distribution function.

C. Unavailability of Overhead Distribution Lines

To assess the impact of an earthquake with a given maximum horizontal ground acceleration, the probability associated with different states of structural damage should be first quantified. In this paper, fragility curves for different elements are defined corresponding to five states of damage introduced earlier. Different fragility curves for distribution overhead lines are demonstrated in Fig. 4. The probability corresponding to each state of damage is evaluated as follows:

$$P(N|G_a) = P_N + P_{Sl} + P_M + P_E + P_C = 1 \quad (3)$$

$$P(Sl|G_a) = P_{Sl} + P_M + P_E + P_C \quad (4)$$

$$P(M|G_a) = P_M + P_E + P_C \quad (5)$$

$$P(E|G_a) = P_E + P_C \quad (6)$$

$$P(C|G_a) = P_C \quad (7)$$

$$P_E = P[E|G_a] - P[C|G_a] \quad (8)$$

$$P_M = P[M|G_a] - P[E|G_a] \quad (9)$$

$$P_{Sl} = P[Sl|G_a] - P[E|G_a] \quad (10)$$

$$P_N = 1 - P[N|G_a] \quad (11)$$

where the letters N , Sl , M , E , and C respectively stand for none, slight, moderate, extensive and complete-damage states of a grid element following a HILP earthquake. In (3)–(7), the cumulative probability of each damage state is calculated based

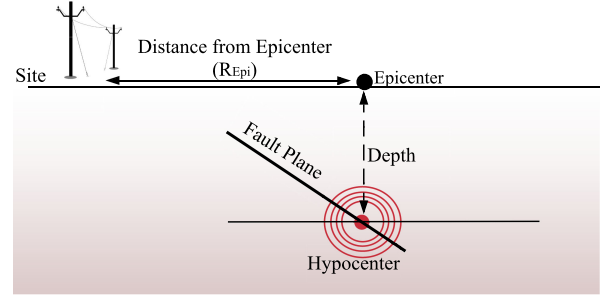


Fig. 3. Illustration of R_{Epi} ; the distance between the epicenter of the earthquake and a location of interest.

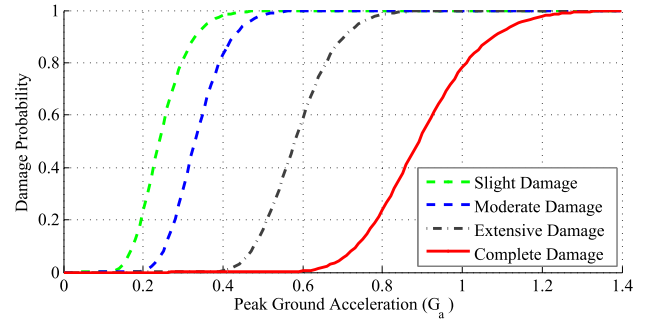


Fig. 4. The fragility curves of power distribution lines.

on the PGA value, while the individual probability of each state of damage is assessed using (8)–(11). Accordingly, the unavailability of each line section in distribution network can be expressed as:

$$lg_{tot} = \sum_k lg_k \quad (12)$$

$$u_{dl_k} = \frac{lg_k}{lg_{tot}} \times [P_{Sl}Q_{Sl} + P_MQ_M + P_EQ_E + P_CQ_C] \quad (13)$$

where, Q_{Sl} , Q_M , Q_E and Q_C denote the failure of 4%, 12%, 50%, and 80% of all distribution lines [56].

In addition to the direct effects of an earthquake on the infrastructure (e.g., the power tower collapses), the indirect effects such as the collapse of the adjacent buildings on distribution overhead lines also contribute to the unavailability of the elements. The fragility curves of the electrical structures adjacent to the buildings are therefore estimated to capture the collapse probability in different states of damage. According to [56], only in cases of extensive and/or complete damage states, a part of the buildings skeletons may be thrown out or would partially collapse which can be translated into an increment in the unavailability of the overhead lines adjacent to such buildings. Furthermore, it can be experimentally demonstrated that the higher the distance between power towers and nearby buildings, the lower the effect of buildings collapse on the overhead lines or power towers. In other words, if the distance between a power tower and an adjacent building is equal to the building height, the effect of the building collapse on the overhead lines could be ignored. In this paper, the impact of a nearby building

collapse on the distribution overhead lines is characterized as follows:

$$F_{dl_k} | F_{bl} = e^{(-\lambda \cdot Dis)}. CP_E(G_a) \quad (14)$$

where, λ is correlated with the building height. Finally, the unavailability of each line section in the distribution network following an earthquake can be defined as in (15):

$$\bar{U}_{dL_k} = u_{dl_k} + P(F_{dl_k} | F_{bl}) - u_{dl_k} \cdot P(F_{dl_k} | F_{bl}) \quad (15)$$

It can be easily discerned that the sections in the vicinity of the adjacent buildings are more vulnerable following an earthquake than those further away.

IV. PROPOSED ALGORITHM FOR RESILIENCE-DRIVEN BESS PLANNING IN POWER DISTRIBUTION SYSTEMS

In this paper, we investigate harnessing the flexibility of the BESS in distribution systems for enhanced resilience against HILP earthquake hazards. Grid hardening via BESS allocation is pursued with the main goal to serve the critical load points during and following the earthquakes. In the following, the proposed algorithmic solution for optimal siting and sizing of BESSs as well as network hardening procedure is presented.

A. Candidate Nodes for BESSs Placement

An earthquake may result in some distribution line sections being unavailable and/or some load points to be interrupted, making it cumbersome, if not impossible, to define a certain operating state for the network following the incident. In order to select the candidate nodes for BESSs placement, we suggest **Algorithm 1**. Indeed, if K represents the total number of distribution line sections, a total number of 2^K states can be experienced. Based on the availability status of each line section, the probability of every possible operating state that the network may reside in following an earthquake can be assessed as follows (**Step 2** and **Step 3**):

$$P_n = \prod_k \left[v_{dl_k} + (\gamma_{dl_k} - v_{dl_k}) \bar{U}_{dL_k} \right] \quad (16)$$

$k = 1, \dots, K; n \in 1 : 2^K$

$$v_{dl_k} + \gamma_{dl_k} = 1 \quad \forall k \quad (17)$$

Each candidate node can host BESS and based on the network configuration, the load curtailment indices can be evaluated. Note that even if a node (nd) hosts a BESS regardless of the size, some critical loads may be disconnected from the main network due to the unavailable distribution line sections (**Step 5**). A Worst Case Index (WCI) defined in (18), is suggested to be evaluated at all load points, representing the amount of critical load curtailment at each node in the most probable network operating state following an earthquake (**Step 6**).

$$WCI_{nd} : LC | \max(P_n) \quad n \in \mathbb{R}, \quad \forall nd \quad (18)$$

Eventually, the selected nodes among all candidate nodes are found as those with the lowest WCI (**Step 9**). This reflects

the fact that considering the network configuration, it is more reasonable to place the BESS in nodes that would better supply the demanded critical loads following an earthquake with more number of available connected line sections.

B. Optimal Sizing of the BESS Solutions

1) *Inputs to the Proposed Optimization Engine*: A power distribution grid will be divided into several islands following a severe HILP disaster. The probability of each islanding scenario can be assessed following the same derivations in (16) and (17) and will be inputted into the optimization model. With the expected amount of critical loads estimated in each scenario, a resilience-driven optimization model is proposed that best finds the BESS sizes across the network (see **Algorithm 2** and **Algorithm 3**).

Algorithm 1: Candidate Node Selection for BESS Siting.

Input: $k, WCI_{nd} = 0$

1: *for* $n = 1 : 2^k$

2: Determine the network configuration.

3: Evaluate the network configuration probability.

4: *for* all nodes (nd) as the candidate nodes:

5: Evaluate the load curtailment (LC) in the network if node (nd) hosts BESS.

6: $WCI_{nd} = WCI_{nd} + P_n \cdot LC$

7: *end for*

8: *end for*

9: **Sort** candidate nodes based on the corresponding WCI_{nd} .

Algorithm 2: Scenario Generation.

Input: $n, N = 2^k$

1: *for* $n = 1 : N$ **Compute**

2: P_n

3: *end for*

4: *for* each possible island in each operating state (n):

5: Compute the value of LC in each island.

6: Determine the location of each BESS in each island.

7: *end for*

8: *for* all of possible islands following an earthquake

9: *for* all possible combination of BESSs

10: Find all system operating states in which the specified combination of BESSs must supply demanded critical loads in the network.

11: Generate scenario s using the associated states.

12: *end for*

13: *end for*

Algorithm 3: Inputs to the Resilience-Driven Optimization.

1: *for* each scenario, **Calculate**

2: The scenario probability.

3: Expected peak critical demand in each island.

4: *end for*

2) *Objective Function*: We first define a metric representing power distribution grid resilience in the face of an earthquake. The main challenge arises from the fact that such HILP events are hard to predict, if not impossible. We assume that the earthquake can happen at each time slot of a day (the earthquake occurrence time (τ) floating between $t = 1$ and $t = 24$)—see Fig. 5; thus, the probability of earthquake occurrence is assumed to be equal to $p_\tau = 1/24$. The objective function is defined as a resilience index (RI) to be maximized:

$$RI = \sum_{\tau=1}^{24} \frac{p_\tau}{D_\tau^{t^e}} \left(\sum_{s=1}^{N_s} p_s \sum_{i=1}^{N I_s} \sum_{t=1}^{t^e} \Delta t \left(\sum_{b=1}^{N_b} \alpha_{(b,s,i)} P_{(b,\tau,s,t)}^{dch} \right) \right) \quad (19)$$

Since there are critical loads that will be interrupted (disconnected from the main grid) during an earthquake and may not be fully supplied even with BESSs, the *RI* index tends to value less than one. Furthermore, a BESS has a certain capacity and can supply one or several critical load points for a limited period of time following an earthquake. This time period, namely emergency response time, is case dependent and extremely driven by network configuration and emergency actions run by the system operators (e.g., using transferable transformers). Emergency response time can be estimated using historical records and past experiences and may last from one to several hours. The proposed *RI* metric is actually the ratio of the BESSs discharge energy during the emergency time interval to the demanded energy by the critical loads over different scenarios. The *RI* metric should encapsulate different scenarios capturing the internal (e.g., critical load profiles) and external HILP-driven uncertainties (e.g., location, time, and severity). The index is embedded in an optimization engine that offers the BESSs optimal solutions that are robust to uncertainties and help to achieve maximum supply and recovery of critical loads following an earthquake.

3) *Optimization Constraints*: The linear programming (LP) optimization problem is subject to several constraints which are formulated as follows:

$$0 \leq \sum_{b=1}^{N_b} \alpha_{(b,s,i)} P_{(b,\tau,s,t)}^{dch} \leq L_{(\tau,s,i,t)} \quad \forall \tau, s, i, t \quad (20)$$

$$0 \leq P_{(b,\tau,s,t)}^{dch} \leq P_b^{max} \quad \forall b, \tau, s, t \quad (21)$$

$$0 \leq E_{(b,\tau)}^{max} \leq E_b^{max} \quad (22)$$

$$0 \leq \sum_{b=1}^{N_b} P_b^{max} \leq \max \left(\sum_{lp=1}^{N_{lp}} L_{(lp,t)} \right) \quad \forall t = 1 : 24 \quad (23)$$

$$0 \leq \sum_{b=1}^{N_b} E_b^{max} \leq \max \left(\sum_{lp=1}^{N_{lp}} E_{(lp,t)}^{t^e} \right) \quad \forall t = 1 : 24 \quad (24)$$

$$E_{(b,\tau,s,t+1)} = E_{(b,\tau,s,t)} - P_{(b,\tau,s,t)}^{dch} \Delta t / \eta_b^{dch} \quad \forall b, \tau, s, t \quad (25)$$

$$E_{(b,\tau,s,t=0)} = E_{(b,\tau)}^{max} \quad \forall b, \tau, s \quad (26)$$

$$C^f + \sum_{b=1}^{N_b} [C^p P_b^{max} + C^E E_b^{max}] \leq \bar{C} \quad (27)$$

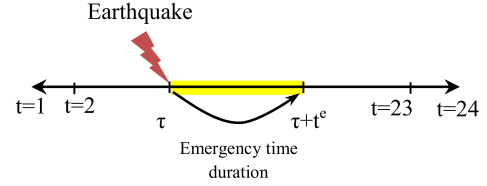


Fig. 5. Illustration of the random timing (τ) for a HILP earthquake in a 24-hour time period and the emergency response time (t^e) following the event.

In each scenario, the total discharge of all BESSs in every island is limited by the critical power in (20). Constraints (21) and (22) enforce the BESS discharge power and state-of-charge (SOC) limits. Inequality (23) limits the sum of maximum discharge power of BESSs to the total critical loads in all time steps. Constraint (24) indicates that the sum of SOC for all BESSs is limited by the maximum critical energy during the emergency response time that varies from 1 to 24 hours (see Fig. 5). The relationship between BESS discharging power and the SOC is illustrated in (25). Equality constraint (26) sets the initial SOC to its maximum value. Finally, constraint (27) enforces a budget limit for BESS deployment in the grid. The optimization engine finds the optimal decision variables (P_b^{max} and E_b^{max}) that maximize the *RI* metric.

C. Network Hardening Solution

The proposed process for network hardening via BESS can be summarized as follows:

- 1) Estimation of PGA at the location of electric facilities and power equipment through AR.
- 2) Probability assessment of different damage states based on statistical fragility curves and the evaluated PGA at the location of power equipment.
- 3) Assessment of the availability of distribution line sections based on (3)–(15).
- 4) Selection of the network candidate nodes for BESSs placement using a proposed *WCI* metric.
- 5) Generation of all possible operating scenarios (Algorithm 2).
- 6) Assessment of the scenario probabilities using (16) and expected peak load at the critical load points in each scenario (Algorithm 3).
- 7) Characterizing a resilience metric based on demanded critical energy during the emergency time—see (19).
- 8) Implementation of a linear optimization formulation to find the optimal size of BESS considering the allocated budget for network hardening against earthquakes.

V. NUMERICAL CASE STUDY AND SIMULATION RESULTS

A. Seismic Considerations and Data Resources

Iran is one of the most seismic countries in the world which includes three seismic zones of Zagros, Alborz, and central Iran [55]. Among the several past destructive earthquakes occurred in Iran, the ones with 7.7 Richter in Tabas in 1978, the 7.2

Richter in Rudbar-Manjil in 1990, the 6.7 Richter in Bam in 2003, and the 7.3 Richter in Kermanshah in 2017 can be highlighted [57]. The capital Tehran's metropolitan area is equipped with advanced energy infrastructures that are potentially threatened by HILP earthquakes. In order to mathematically model a seismic hazard and assess the seismic vulnerability of power equipment, historical catalogues are accessed based on the available information from different sources: data on the earthquakes as old as 400 BC is gathered from [58] which contains references to 256 pre-1900 historical earthquakes in Iran. For post 1900 events, the data in [59]–[63] have been utilized. Based on the provided historical catalogues for Tehran's seismic vulnerability, one can realize that during the last century, no strong event was located near Tehran, but several earthquakes of moment magnitude greater than 5 occurred and were associated with the Mosha, the Ipak, and the North Alborz faults, north and south Ray fault. According to [64], 84,000 earthquakes of magnitude 4.6–7.55 representing full temporal and spatial distributions of 10,000 years of earthquakes in an area of 200 km radius from Tehran are generated using Monte-Carlo Simulations (MCS). In [64], it is assessed that among the numerous earthquake scenarios, the most probable earthquake for Tehran is a hazard with moment magnitude of 6.75 and return period of 475-years. According to Iranian seismic design code-Standard 2800 [65], Tehran has not experienced a strong earthquake for 180 years, and as such, we here assumed that the most probable earthquake in Tehran would have a moment magnitude of 6.75 as well [64].

According to [55], the main ground type in Iran is mostly rock and soil, based on which, the soil type at the location of the test case in Tehran is considered as rock. According to the Iranian code of practice for seismic-resistant design of buildings [65], one may consider the rock type equivalent to shear wave velocities higher or equal to 375 m/s and the soil type equivalent to shear wave velocities are less than 375 m/s. Motivated by [55], the specific attenuation relationship (AR) used in this study is described as follows:

$$\ln(G_a) = C_1 + C_2 \left(\frac{M_W + 0.38}{1.06} \right) + C_3 \ln [R] \quad (28)$$

As the ground type in the test case is of rock [65], the seismic constant coefficients, C_1 , C_2 and C_3 are 4.15, 0.623, and -0.96 , respectively.

B. Test System Considerations and Assumptions

The proposed resilience-driven BESSs framework is implemented on a medium-voltage distribution feeder in Tehran, the geotechnical vulnerability map of which is demonstrated in Fig. 6 and its simplified single-line diagram is illustrated in Fig. 7. According to Fig. 6, one can realize that the main feeder under study is located in areas that are identified with medium and high geotechnical risk and vulnerability levels. This feeder contains six critical load points. The load profile forecasts are taken for a typical day in July 2018, presented in Fig. 8 with the peak load values tabulated in Table I. It is assumed that the focused distribution feeders are disconnected from the mainstream

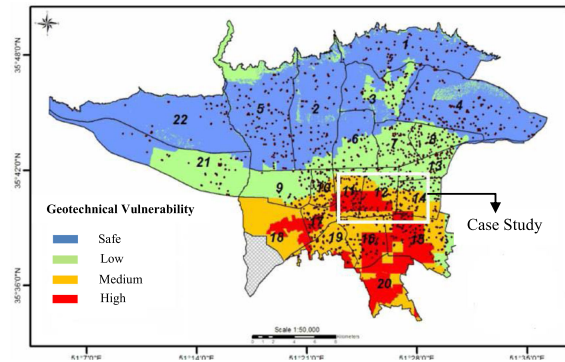


Fig. 6. The geotechnical vulnerability map of the studied network in the Tehran metropolitan area, Iran.

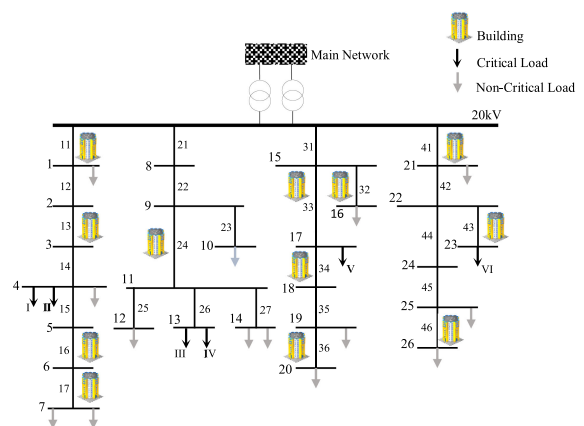


Fig. 7. The simplified diagram of one main distribution feeder in Tehran.

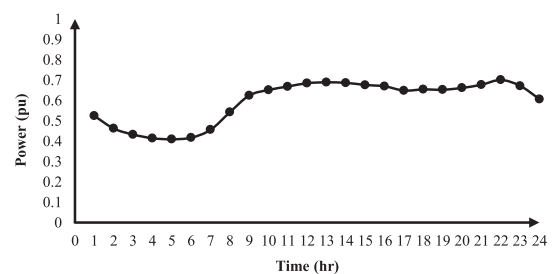


Fig. 8. Forecasted load profiles of critical load points.

TABLE I
FORECASTED PEAK VALUES OF CRITICAL LOADS

Load Point	I	II	III	IV	V	VI
Power (kW)	368.8	418	410.8	520.7	532.5	454.5

following an earthquake. The emergency response time is supposed to be 10 hours captured from the 2003 Bam earthquake historical data [66]. The distance between the nearby building and the overhead lines is considered 5 meters. In addition, the buildings in the vicinity of the overhead lines are considered 20 or 45 meters high, and their structures are concrete or steel with the fragility curves borrowed from [56]. The seismic

TABLE II
MEDIAN AND LOGNORMAL STANDARD DEVIATION OF DIFFERENT
DAMAGE STATES

Damage State	Median (g)	β
Slight	0.24	0.25
Moderate	0.33	0.20
Extensive	0.58	0.15
Complete	0.89	0.15

TABLE III
FRAGILITY RESULTS FOR DIFFERENT DAMAGE STATES WHEN $PGA = 0.6 G$

Damage State	Damage Accumulative Probability	Damage State Probability
None	1	0
Slight	1	0.0014
Moderate	0.9986	0.413487
Extensive	0.5894	0.585113
Complete	0.0043	0.0043

TABLE IV
UNAVAILABILITY OF LINE SECTIONS FOLLOWING AN EARTHQUAKE

Line section	U_{ds}	Line section	U_{ds}	Line section	U_{ds}
11	0.3700396	23	0.0325555	35	0.0237342
12	0.0076903	24	0.32933752	36	0.32477745
13	0.1823717	25	0.02604438	41	0.36521764
14	0.0192257	26	0.0208065	42	0.0100712
15	0.0239253	27	0.18629466	43	0.18541105
16	0.1943316	31	0.01309961	44	0.03521399
17	0.1898610	32	0.3807675	45	0.0194381
21	0.0315301	33	0.40110888	46	0.37263095
22	0.0131589	34	0.20581798		

standards have generally categorized the buildings into four key levels of high-code, moderate-code, low-code, and not seismically designed [56], and we assumed the focused buildings in this study are of the moderate-code seismic category. Furthermore, the BESSs are considered to be of a lithium-ion type. The BESS fixed and variable installation costs are assumed 1 M\$, 175 \$/kW (power), and 500 \$/kWh (energy), respectively [67]. The BESS discharge efficiency is assumed 85% and the total budget for BESS deployment in the network is 5 M\$.

C. Numerical Results, Sensitivity Analyses, and Discussions

The methodology employed in this paper to assess the failure probability of distribution line sections was developed by FEMA. According to [56], the medians and lognormal standard deviation of fragility curves used for different damage states are expressed in Table II. If the estimated PGA at the location of the distribution line section is found 0.6g, the probability of different damage states are tabulated in Table III based on equations (3)–(11). The unavailability of each line section is assessed in Table IV. As can be seen, the buildings close to the overhead lines contribute to the lines' unavailability following an earthquake. The proposed candidate node selection algorithm for BESS sitting is applied to the studied test case. The detailed

TABLE V
THE CALCULATED WCI INDEX FOR CANDIDATE NODES

Node Number	1	2	3	4	8
WCI index (kW)	1918.5	1918.5	1918.5	1918.5	1319.3
Node Number	9	11	13	15	17
WCI index (kW)	1319.3	1773.8	1773.8	1319.3	2172.8
Node Number	21	22	23		
WCI index (kW)	2250.9	2250.9	2250.9		

TABLE VI
EXPECTED CRITICAL DEMAND FOR DIFFERENT ISLANDING SCENARIOS

Scenario (s)	p_s	Partitioned-Network Solutions		
		No. of Island	Expected Peak Critical Demand	Storages Number
1	0.000017392	1	828.814741	1
2	0.000844872	1	931.548600	2
3	0.010359045	1	1012.495418	3
4	0.006678507	1	1221.121869	1,2
5	0.003896017	1	1048.340069	1,3
6	0.911589947	1	1611.758940	1,2,3
7	0.00003327	1	828.814741	1
		2	931.548600	2
8	0.000025967	1	828.814741	1
		2	532.522300	3
9	0.000260765	1	931.548600	2
		2	1012.495418	3
10	0.025228494	1	904.572783	3
		2	1046.002895	1,2
11	0.007452983	1	931.548600	2
		2	1048.340069	1,3
12	0.000049674	1	828.814741	1
		2	931.548600	2
		3	532.522300	3

TABLE VII
OPTIMAL SIZE OF THE ALLOCATED BESS IN DISTRIBUTION NETWORK

RI	E_1^{max} (kWh)	P_1^{max} (kW)	E_2^{max} (kWh)	P_2^{max} (kW)	E_3^{max} (kWh)	P_3^{max} (kW)
0.40	1093	93	2073	176	4603	391

numerical results on the evaluated WCI for all nodes are displayed in Table V. As it can be seen, the suitable nodes are those that, if hosting the BESS, result in the minimum load curtailment in the network following an earthquake. Therefore, $BESS^1$, $BESS^2$ and $BESS^3$ are respectively placed in nodes 8, 9, and 15, resulting in the least value of load curtailment (=1319.348 kW). Following an earthquake, the distribution network will be partitioned into several islands introduced in Table VI. The BESSs should supply the critical loads in each island during the emergency response interval. Scenarios (S) are generated, and it is observed that S6 is the most feasible in which all the three BESSs can supply the critical loads. Other scenarios such as S3 and S10 also contribute to the decision on the optimal size of the BESSs. The proposed optimization problem is solved, and the optimal size of BESSs is determined as summarized in Table VII. One can see that the power and

TABLE VIII
RESILIENCE INDEX AS A FUNCTION OF EMERGENCY RESPONSE TIME

Emergency Response Time (hr)	RI	E_1 (kWh)	P_1 (kW)	E_2 (kWh)	P_2 (kW)	E_3 (kWh)	P_3 (kW)
8	0.483958	886.771	118.425	2771.584	294.481	3999.402	564.932
9	0.439875	1045.047	98.699	2188.818	206.722	4487.677	490.172
10	0.397347	1092.692	92.879	2072.918	176.198	4603.248	391.330
11	0.361577	1201.961	92.879	1523.101	117.694	5064.272	391.330
12	0.331722	1311.230	92.879	970.574	68.749	5524.660	391.330
13	0.306434	1420.499	92.879	415.471	27.165	5985.049	391.330
14	0.28474	1404.076	85.247	0	0	6429.122	391.330
15	0.265911	968.297	54.870	0	0	6875.533	391.330
16	0.249401	487.752	25.912	0	0	7366.214	391.330

TABLE IX
RESILIENCE INDEX AS A FUNCTION OF THE MARGINAL BUDGET FOR GRID HARDENING

Marginal Budget (M\$)	RI	E_1 (kWh)	P_1 (kW)	E_2 (kWh)	P_2 (kW)	E_3 (kWh)	P_3 (kW)
2	0.099606	0	0	0	0	1942.219	165.089
4	0.29844	1092.692	92.879	130.082	11.057	4603.884	391.330
6	0.489917	1133.992	133.379	3093.770	297.656	5404.520	619.585
8	0.533417	1071.453	100.004	6070.351	632.927	6379.572	634.565
10	0.575667	2132.214	201.376	7360.742	654.261	7959.264	709.452
12	0.575667	2132.214	201.376	7360.742	654.261	7959.264	709.452

energy provided by $BESS^3$ is higher than the others: $BESS^1$ should supply an expected peak critical load of 828.81 kW in S1, S7, S8, and S12 (with the probability of 0.0001), $BESS^2$ should supply 931.55 kW of load in S7, S9, S11, and S12 (with the probability of 0.0086) and finally $BESS^3$ supplies an expected peak critical load of 935.69 kW in S3, S8, S9, S10, and S12 (with the probability of 0.0359). The additional flexibility provided by BESSs has improved the resilience index by 40%.

1) *Sensitivity Analysis on Emergency Response Time*: According to Table VIII, one can see that as the emergency response time increases, the resilience index will decrease since the marginal budget (\bar{C}) is set fixed to 5M\$. As the emergency response time increases, the estimated energy level of the $BESS^1$ and $BESS^2$ will be almost zero and $BESS^3$ will be the only unit with a high nominal energy level in the system. This is because S3 and S10 (with the probabilities of 0.01 and 0.025, respectively) are the most probable scenarios following S6 and $BESS^3$ should supply 904.57 kW and 1012.5 kW of the system critical loads correspondingly. Therefore, according to Fig. 9, it is expected that with a fixed hardening budget and an emergency response time longer than 16 hours, $BESS^3$ is the only unit with a significant role in deriving the network resilience.

2) *Sensitivity Analysis on the Marginal Budget for Grid Hardening With BESS*: If the emergency response time is considered equal to 10 hours, the changes in the resilience index and power and energy size of the BESS corresponding to different marginal budgets for grid hardening are illustrated in Table IX. In the most probable scenario (i.e., S6), Table VI reflects that all the BESSs should be connected to the main network and should supply the system demanded critical loads. $BESS^3$ with the probability of 0.0359, $BESS^2$ with the probability of 0.0086,

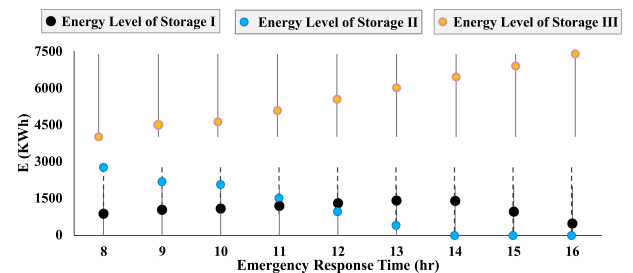


Fig. 9. Energy level of BESSs as a function of emergency response time.

and $BESS^1$ with the probability of 0.0001 should supply demanded critical loads in all other scenarios except S6. Therefore, one can realize from the results that as the marginal budget (\bar{C}) increases, the $BESS^3$ is the only storage unit which plays a significant role on enhancing the network resilience and, as a result, it should be characterized with a higher energy level, $E(kWh)$, compared to $BESS^2$ and $BESS^1$. According to Table IX, one can see that the resilience index and the energy and power level of the BESS do not change with the marginal budgets higher than 10 (M\$) and the system resilience cannot be further improved. In the best scenario, the maximum resilience is found 0.576, simply meaning that 57.6% of the demanded critical energy in the network can be supplied during the emergency time following a seismic hazard in Tehran. One remarkable feature of the proposed optimization is that the solution is found in an automated manner and after a single run, since the optimization engine is designed linear; thus, the optimization problem is not only able to find the global optimal results, but also is characterized with an acceptable computational time as compared to the heuristic or nonlinear optimization models.

VI. CONCLUSION

This paper investigates the feasibility of BESSs deployment in power distribution systems to improve its resilience against HILP incidents in general and earthquakes in particular. The proposed model first characterizes the earthquake hazards, then suggests a grid vulnerability assessment mechanism and eventually presents a methodology for BESS siting and sizing for enhanced resilience. In the first stage, a large historical earthquake dataset was employed to estimate the potential seismic intensity and an analytical attenuation relationship was utilized to characterize the seismic hazard via the peak ground acceleration at the location of interest. In the second stage, an effective application of fragility curves was pursued in order to assess the grid vulnerability and estimate the impact of a seismic hazard on the availability of distribution line sections, where the failure of power distribution equipment such as towers and overhead line sections due to external forces (e.g. the collapse of adjacent buildings) was also modeled. In the third stage, a quantitative criterion was suggested that helps finding the candidate nodes in the network to host the BESS. An LP optimization based on a new resilience metric was formulated to find the optimal capacity of the BESS units across the network. The proposed hardening framework was implemented on a real-world distribution feeder in Tehran, Iran, and the results were extensively analyzed. Numerical results revealed that the BESS flexibility, if effectively harnessed, could help in supplying the critical loads during and following the earthquakes. This study can also help the system planners and decision makers in allocating the required budget to harden the network robustness with BESSs, aiming at an enhanced resilience against catastrophic HILP hazards.

REFERENCES

- [1] P. Southwell, "Disaster recovery within a CIGRE strategic framework: Network resilience, trends and areas of future work," *SC C1 CIGRE Tech. Committee*, 2014.
- [2] S. Espinoza, M. Panteli, P. Mancarella, and H. Rudnick, "Multi-phase assessment and adaptation of power systems resilience to natural hazards," *Electric Power Syst. Res.*, vol. 136, pp. 352–361, 2016.
- [3] A. M. Salman, Y. Li, and M. G. Stewart, "Evaluating system reliability and targeted hardening strategies of power distribution systems subjected to hurricanes," *Rel. Eng. Syst. Saf.*, vol. 144, pp. 319–333, 2015.
- [4] A. Kocatepe, M. B. Ulak, L. M. K. Sriram, D. Pinzan, E. E. Ozguven, and R. Arghandeh, "Co-resilience assessment of hurricane-induced power grid and roadway network disruptions: A case study in Florida with a focus on critical facilities," in *Proc. 21st Int. Conf. Intell. Transp. Syst.*, 2018, pp. 2759–2764.
- [5] *U.S. Energy Information Administration Report*. 2017. [Online]. Available: <https://www.eia.gov/todayinenergy/detail.php?id=32892>
- [6] *U.S. Energy Information Administration Report*. 2017. [Online]. Available: <https://www.eia.gov/todayinenergy/detail.php?id=32992>
- [7] Council of Economic Advisers, *Economic Benefits of Increasing Electric Grid Resilience to Weather Outages*. The White House, Washington, DC, USA, 2013.
- [8] B. Zhang, P. Dehghanian, and M. Kezunovic, "Optimal allocation of PV generation and battery storage for enhanced resilience," *IEEE Trans. Smart Grid*, vol. 10, no. 1, pp. 535–545, Jan. 2019.
- [9] P. Dehghanian, *Power System Topology Control for Enhanced Resilience of Smart Electricity Grids*. Ph.D. dissertation, Dept. Elect. Comput. Eng., Texas A&M Univ., College Station, College Station, TX, USA, 2017.
- [10] R. Billinton, *Power System Reliability Evaluation*. Abingdon, UK: Taylor & Francis, 1970.
- [11] X. Liu, M. Shahidepour, Z. Li, X. Liu, Y. Cao, and Z. Bie, "Microgrids for enhancing the power grid resilience in extreme conditions," *IEEE Trans. Smart Grid*, vol. 8, no. 2, pp. 589–597, Mar. 2017.
- [12] S. Chanda and A. K. Srivastava, "Defining and enabling resiliency of electric distribution systems with multiple microgrids," *IEEE Trans. Smart Grid*, vol. 7, no. 6, pp. 2859–2868, Nov. 2016.
- [13] M. Panteli, C. Pickering, S. Wilkinson, R. Dawson, and P. Mancarella, "Power system resilience to extreme weather: Fragility modelling, probabilistic impact assessment, and adaptation measures," *IEEE Trans. Power Syst.*, vol. 32, no. 5, pp. 3747–3757, Sep. 2017.
- [14] W. Zeng, Y. Zhang, and M.-Y. Chow, "Resilient distributed energy management subject to unexpected misbehaving generation units," *IEEE Trans. Ind. Inform.*, vol. 13, no. 1, pp. 208–216, Feb. 2017.
- [15] P. Li, Y. Liu, H. Xin, and X. Jiang, "A robust distributed economic dispatch strategy of virtual power plant under cyber-attacks," *IEEE Trans. Ind. Inform.*, vol. 14, no. 10, pp. 4343–4352, Oct. 2018.
- [16] G. P. Cimellaro, A. M. Reinhorn, and M. Bruneau, "Framework for analytical quantification of disaster resilience," *Eng. Struct.*, vol. 32, no. 11, pp. 3639–3649, 2010.
- [17] D. Henry and J. E. Ramirez-Marquez, "Generic metrics and quantitative approaches for system resilience as a function of time," *Rel. Eng. Syst. Saf.*, vol. 99, pp. 114–122, 2012.
- [18] M. Ouyang and L. Duenas-Osorio, "Multi-dimensional hurricane resilience assessment of electric power systems," *Structural Saf.*, vol. 48, pp. 15–24, 2014.
- [19] *Critical Infrastructure Security and Resilience*. White House, 2013.
- [20] M. Panteli and P. Mancarella, "Influence of extreme weather and climate change on the resilience of power systems: Impacts and possible mitigation strategies," *Electric Power Syst. Res.*, vol. 127, pp. 259–270, 2015.
- [21] M. Panteli and P. Mancarella, "The grid: Stronger, bigger, smarter?: Presenting a conceptual framework of power system resilience," *IEEE Power Energy Mag.*, vol. 13, no. 3, pp. 58–66, May/Jun. 2015.
- [22] M. Panteli, P. Mancarella, D. N. Trakas, E. Kyriakides, and N. D. Hatziargyriou, "Metrics and quantification of operational and infrastructure resilience in power systems," *IEEE Trans. Power Syst.*, vol. 32, no. 6, pp. 4732–4742, Nov. 2017.
- [23] F. Petit, R. Fisher, and S. Veselka, "Resiliency measurement index," Argonne, IL, USA: Argonne Nat. Lab., USA, Tech. Rep. ANL/DIS-13-01, 2013.
- [24] Y. Wang, C. Chen, J. Wang, and R. Baldick, "Research on resilience of power systems under natural disasters—A review," *IEEE Trans. Power Syst.*, vol. 31, no. 2, pp. 1604–1613, Nov. 2016.
- [25] K. P. Schneider, F. K. Tuffner, M. A. Elizondo, C.-C. Liu, Y. Xu, and D. Ton, "Evaluating the feasibility to use microgrids as a resiliency resource," *IEEE Trans. Smart Grid*, vol. 8, no. 2, pp. 687–696, Mar. 2017.
- [26] M. Simonov, "Dynamic partitioning of dc microgrid in resilient clusters using event-driven approach," *IEEE Trans. Smart Grid*, vol. 5, no. 5, pp. 2618–2625, Sep. 2014.
- [27] J. Lai, X. Lu, F. Wang, P. Dehghanian, and R. Tang, "Broadcast gossip algorithms for distributed peer-to-peer control in ac microgrids," *IEEE Trans. Industry Appl.*, in press, 2019.
- [28] H. Farzin, M. Fotuhi-Firuzabad, and M. Moeini-Aghtaie, "Enhancing power system resilience through hierarchical outage management in multi-microgrids," *IEEE Trans. Smart Grid*, vol. 7, no. 6, pp. 2869–2879, Nov. 2016.
- [29] C. Chen, J. Wang, F. Qiu, and D. Zhao, "Resilient distribution system by microgrids formation after natural disasters," *IEEE Trans. Smart Grid*, vol. 7, no. 2, pp. 958–966, Mar. 2016.
- [30] A. Sharma, D. Srinivasan, and A. Trivedi, "A decentralized multiagent system approach for service restoration using DG islanding," *IEEE Trans. Smart Grid*, vol. 6, no. 6, pp. 2784–2793, Nov. 2015.
- [31] Z. Wang and J. Wang, "Self-healing resilient distribution systems based on sectionalization into microgrids," *IEEE Trans. Power Syst.*, vol. 30, no. 6, pp. 3139–3149, Nov. 2015.
- [32] P. Dehghanian, B. Zhang, T. Dokic, and M. Kezunovic, "Predictive risk analytics for weather-resilient operation of electric power systems," *IEEE Trans. Sustain. Energy*, vol. 10, no. 1, pp. 3–15, Jan. 2019.
- [33] P. Dehghanian, S. Aslan, and P. Dehghanian, "Quantifying power system resiliency improvement using network reconfiguration," in *Proc. IEEE 60th Int. Midwest Symp. Circuits Syst.*, 2017, pp. 1–6.
- [34] W. Bakun *et al.*, "Implications for prediction and hazard assessment from the 2004 Parkfield earthquake," *Nature*, vol. 437, no. 7061, pp. 969–974, 2005.
- [35] N. R. Romero, L. K. Nozick, I. D. Dobson, N. Xu, and D. A. Jones, "Transmission and generation expansion to mitigate seismic risk," *IEEE Trans. Power Syst.*, vol. 28, no. 4, pp. 3692–3701, Nov. 2013.
- [36] I. Vanzi, "Structural upgrading strategy for electric power networks under seismic action," *Earthquake Eng. Structural Dyn.*, vol. 29, no. 7, pp. 1053–1073, 2000.

- [37] Y. Shumuta, "Practical seismic upgrade strategy for substation equipment based on performance indices," *Earthquake Eng. Structural Dyn.*, vol. 36, no. 2, pp. 209–226, 2007.
- [38] S. Espinoza *et al.*, "Seismic resilience assessment and adaptation of the Northern Chilean power system," in *Proc. IEEE Power Energy Soc. General Meeting*, 2017, pp. 1–5.
- [39] A. Poulos, S. Espinoza, J. de la Llera, and H. Rudnick, "Seismic risk assessment of spatially distributed electric power systems," presented at the *16th World Conf. Earthquake Eng.*, Santiago, Chile, 2017.
- [40] J. Buritica, S. Tesfamariam, and M. Sánchez-Silva, "Seismic vulnerability assessment of power transmission networks using complex-systems based methodologies," in *Proc. 15th World Conf. Earthquake Eng.*, 2012, pp. 24–28.
- [41] J. A. Buriticá Cortés, M. Sánchez-Silva, and S. Tesfamariam, "A hierarchy-based approach to seismic vulnerability assessment of bulk power systems," *Struct. Infrastructure Eng.*, vol. 11, no. 10, pp. 1352–1368, 2015.
- [42] K. Poljanšek, F. Bono, and E. Gutiérrez, "Seismic risk assessment of interdependent critical infrastructure systems: The case of European gas and electricity networks," *Earthquake Eng. Structural Dyn.*, vol. 41, no. 1, pp. 61–79, 2012.
- [43] A. M. Salman and Y. Li, "A probabilistic framework for seismic risk assessment of electric power systems," *Procedia Eng.*, vol. 199, pp. 1187–1192, 2017.
- [44] M. Shinozuka, T.-C. Cheng, M. Feng, and S.-T. Mau, "Seismic performance analysis of electric power systems," *Res. Prog. Accomplishments 1997–1999*, pp. 61–69, 1999.
- [45] M. Shinozuka, X. Dong, X. Jin, and T. Cheng, "Seismic performance analysis for the LADWP power system," in *Proc. IEEE/PES Transmiss. Distribution Conf. Exh.: Asia Pacific*, 2005, pp. 1–6.
- [46] M. Shinozuka, X. Dong, T. Chen, and X. Jin, "Seismic performance of electric transmission network under component failures," *Earthquake Eng. Structural Dyn.*, vol. 36, no. 2, pp. 227–244, 2007.
- [47] T. Adachi and B. R. Ellingwood, "Comparative assessment of civil infrastructure network performance under probabilistic and scenario earthquakes," *J. Infrastructure Syst.*, vol. 16, no. 1, pp. 1–10, 2010.
- [48] A.-S. Ang, J. Pires, and R. Villaverde, "A model for the seismic reliability assessment of electric power transmission systems," *Rel. Eng. Syst. Saf.*, vol. 51, no. 1, pp. 7–22, 1996.
- [49] M. Shinozuka, A. Rose, and R. Eguchi, "Engineering and socioeconomic impact of earthquakes: An analysis of electricity lifeline disruptions in the new madrid area monograph 2," in *Multidisciplinary Center for Earthquake Engineering Research, Red Jacket Quadrangle*, Buffalo, NY, USA: State Univ. New York at Buffalo, vol. 14261, 1998.
- [50] T. Adachi and B. R. Ellingwood, "Serviceability of earthquake-damaged water systems: Effects of electrical power availability and power backup systems on system vulnerability," *Rel. Eng. Syst. Saf.*, vol. 93, no. 1, pp. 78–88, 2008.
- [51] T. Anagnos, *Development of an Electrical Substation Equipment Performance Database for Evaluation of Equipment Fragilities*. Pac. Earthquake Eng. Res. Center, Univ. California, Berkeley, CA, USA, 1999.
- [52] M. Panteli, D. N. Trakas, P. Mancarella, and N. D. Hatziargyriou, "Power systems resilience assessment: Hardening and smart operational enhancement strategies," *Proc. IEEE*, vol. 105, no. 7, pp. 1202–1213, Jul. 2017.
- [53] P. Dehghanian, S. Aslan, and P. Dehghanian, "Maintaining electric system safety through an enhanced network resilience," *IEEE Trans. Ind. Appl.*, vol. 54, no. 5, pp. 4927–4937, Sep./Oct. 2018.
- [54] M. Panteli, D. N. Trakas, P. Mancarella, and N. D. Hatziargyriou, "Boosting the power grid resilience to extreme weather events using defensive islanding," *IEEE Trans. Smart Grid*, vol. 7, no. 6, pp. 2913–2922, Nov. 2016.
- [55] G. G. Amiri, A. Mahdavian, and F. M. Dana, "Attenuation relationships for Iran," *J. Earthquake Eng.*, vol. 11, no. 4, pp. 469–492, 2007.
- [56] Federal Emergency Management Agency (FEMA), "Multi-hazard loss estimation methodology: Earthquake model," Department of Homeland Security, FEMA, Washington, DC, 2003.
- [57] M. Zare, F. Kamranzad, I. Parcharidis, and V. Tsironi, "Preliminary report of Mw7.3 Sarpol-e Zahab, Iran earthquake on November 12, 2017," EMSC Report, pp. 1–10, 2017.
- [58] N. Ambraseys and C. Melville, *A History of Persian Earthquakes*. New York, NY, USA: Cambridge Univ. Press, 1982.
- [59] N. Ambraseys and C. Melville, "The catalogue of persian earthquakes," Imperial College of Sci. Technol., Univ. London, U.K., Tech. Rep. 1996.
- [60] I. Asudeh, "ISC mislocation of earthquakes in Iran and geometrical residuals," *Tectonophysics*, vol. 95, no. 1–2, pp. 61–74, 1983.
- [61] B. Tavakoli and M. Ghafory-Ashtiany, "Seismic hazard assessment of Iran," *Ann. Geophys.*, vol. 42, no. 6, pp. 1013–1021, 1999.
- [62] M. Berberian, *Natural Hazards and the First Earthquake Catalogue of Iran*. Tehran, Iran: International Institute of Earthquake Engineers and Seismology, 1994.
- [63] A. Ansari, A. Noorzad, and H. Zafarani, "Clustering analysis of the seismic catalog of Iran," *Comput. Geosci.*, vol. 35, no. 3, pp. 475–486, 2009.
- [64] M. R. Zolfaghari and E. Peyghaleh, "Development of optimization-based probabilistic earthquake scenarios for the city of Tehran," *Comput. Geosci.*, vol. 86, pp. 129–145, 2016.
- [65] *Iranian Code of Practice for Seismic Resistant Design of Buildings*, I. S. Code Standard 2800, 2005.
- [66] Y. Fialko, D. Sandwell, M. Simons, and P. Rosen, "Three-dimensional deformation caused by the Bam, Iran, earthquake and the origin of shallow slip deficit," *Nature*, vol. 435, no. 7040, pp. 295–299, 2005.
- [67] S. M. Schoenung and W. V. Hassenzahl, "Long-vs. short-term energy storage technologies analysis: A life-cycle cost study: A study for the DOE energy storage systems program," SAND2003-2783, Sandia National Laboratories, USA, 2003.

Mostafa Nazemi (S'18) received the B.Sc. degree in electrical engineering from the K. N. Toosi University of Technology, Tehran, Iran, in 2015, and the M.Sc. degree in energy systems engineering from the Sharif University of Technology, Tehran, Iran, in 2017. He is currently pursuing the Ph.D. degree in electrical engineering with the Department of Electrical and Computer Engineering, George Washington University, Washington, DC, USA. His research interests include power system resilience, power system planning and operation, energy optimizations, and smart electricity grid applications.

Moein Moeini-Aghtaie (M'15) received the M.Sc. and Ph.D. degrees in electrical engineering from the Sharif University of Technology, Tehran, Iran, in 2010 and 2014, respectively. He is currently an Assistant Professor with the Department of Energy Engineering, Sharif University of Technology. His current research interests include reliability and resilience studies of modern distribution systems, especially in the multi-carrier energy environment, and charging management of plug-in hybrid electric vehicles.

Mahmud Fotuhi-Firuzabad (F'14) received the Ph.D. degree in electrical engineering from the University of Saskatchewan, Saskatoon, SK, Canada, in 1997. He is currently a Professor and the President of the Sharif University of Technology, Tehran, Iran. Prof. Fotuhi-Firuzabad is a member of the Center of Excellence in Power System Management and Control. He is also an Editor-in-Chief for the IEEE POWER ENGINEERING LETTERS.

Payman Dehghanian (S'11–M'17) received the B.Sc., M.Sc., and Ph.D. degrees in electrical engineering from the University of Tehran, Tehran, Iran, in 2009, Sharif University of Technology, Tehran, Iran, in 2011, and Texas A&M University, Texas, USA, in 2017. He is an Assistant Professor at the Department of Electrical and Computer Engineering in George Washington University, Washington, D.C., USA. His research interests include power system protection and control, power system reliability and resiliency, asset management, and smart electricity grid applications.

Dr. Dehghanian is the recipient of the 2013 IEEE Iran Section Best M.Sc. Thesis Award in electrical engineering, the 2014 and 2015 IEEE Region 5 Outstanding Professional Achievement Awards, and the 2015 IEEE-HKN Outstanding Young Professional Award.